POLITECNICO DI TORINO
Repository ISTITUZIONALE

Impact of Turbulent Inflow on the Far-Field Noise Generated by a Propeller Operating at Low Reynolds Number

Original
Impact of Turbulent Inflow on the Far-Field Noise Generated by a Propeller Operating at Low Reynolds Number / Capobianchi, G., Montagner, S., Piccolo, A., Di Marco, A., Avallone, F., Cafiero, G., Ragni, D., De Paola, E., Stoica, L.G.. - (2024). (30th AIAA/CEAS Aeroacoustics Conference (2024) Rome (ITA) June 4-7, 2024) [10.2514/6.2024-3154].

Availability:
This version is available at: 11583/2989257 since: 2026-03-24T14:25:16Z

Publisher:
American Institute of Aeronautics and Astronautics

Published
DOI:10.2514/6.2024-3154

Terms of use:

This article is made available under terms and conditions as specified in the corresponding bibliographic description in the repository

Publisher copyright
AIAA preprint/submitted version e/o postprint/Author's Accepted Manuscript

(Article begins on next page)

25 November 2026

Impact of turbulent inflow on the far-field noise generated by a propeller operating at low Reynolds number

G. Capobianchi *[1], S. Montagner †[2], A. Piccolo ‡[3], A. Di Marco§[1], F. Avallone ¶[2], G. Cafiero ‖[2], D. Ragni **[3]
E. de Paola ††[1] and L. G. Stoica ‡‡[1]

[1] *Roma Tre University, Department of Civil, Computer Science and Aeronautical Technologies Engineering, Via Vito Volterra, 62, 00146 Rome, Italy.*

[2] *Politecnico di Torino, Department of Mechanical and Aerospace Engineering, Corso Duca degli Abruzzi 24, 10129 Turin, Italy.*

[3] *Delft University of Technology, Faculty of Aerospace Engineering, Kluyverweg 1, 2629 HS Delft, The Netherlands.*

This study analyzes the alteration undergone by turbulent eddies as they approach a propeller operating at low Reynolds number, with the purpose of investigating the resulting effects on the noise emitted by the propeller. The two mechanisms affecting turbulence distortion, the streamtube contraction and the interaction between the turbulent structures and the blade, have been investigated experimentally. The set-up consists of a propeller with a diameter of 30 cm operating at a 75% chord-based Reynolds number of 10.8×10^4 interacting with the turbulence produced by a rectangular grid. The flow behavior has been studied by particle image velocimetry (PIV) and hot-wire anemometry (HWA), while a microphone arc was installed for the acoustic analysis. The results reveal that the interaction between incoming turbulence and the propeller plays a dominant role in the alteration of turbulence with respect to the streamtube contraction. This is due to the relatively low contraction ratio of the propeller at this regime, equal, in this case, to $C.R.$ =1.3. Turbulence characteristics are used as input for two different analytical noise-prediction models, both based on Amiet's theory for turbulence-impingement noise. The first implements the original formulation of Amiet for propeller noise, which requires a position along the blade to be specified to define all the inputs. The second has been developed in the present work to account for the variations of the blade geometry and turbulence conditions in the radial direction. The comparison between the noise predictions and the experimental measurements shows that a better agreement can be obtained with the second model. This reveals that noise generation is strongly dependent on the variation of the flow conditions and propeller geometry along the radial direction, confirming that the description of these characteristics can enhance the accuracy of low-fidelity noise-prediction methods.

I. Nomenclature

BPF	=	blade passing frequency
c	=	reference chord length
CR	=	contraction ratio
$f_\#$	=	f-stop
HWA	=	hot-wire anemometry
I	=	turbulence intensity
L_{ij}^m	=	integral length scale

*PhD student, Roma Tre University, Department of Civil, Computer Science and Aeronautical Technologies Engineering. giorgia.capobianchi@uniroma3.it

†Master student, Politecnico di Torino, Department of Mechanical and Aerospace Engineering.

‡PhD student, Faculty of Aerospace Engineering, Delft University of Technology.

§Associate Professor, Roma Tre University, Department of Civil, Computer Science and Aeronautical Technologies Engineering.

¶Full Professor, Politecnico di Torino, Department of Mechanical and Aerospace Engineering.

‖Associate Professor, Politecnico di Torino, Department of Mechanical and Aerospace Engineering.

**Associate Professor, Faculty of Aerospace Engineering, Delft University of Technology.

††Research fellow, Roma Tre University, Department of Civil, Computer Science and Aeronautical Technologies Engineering.

‡‡Research fellow, Roma Tre University, Department of Civil, Computer Science and Aeronautical Technologies Engineering.

L_{uu}	=	length scale for the streamwise velocity
m	=	direction along which the correlation is calculated
$OASPL$	=	overall sound pressure level
PIV	=	particle image velocimetry
r	=	radial position along the blade
R	=	propeller radius
R_{ij}	=	spatial correlation function
RDT	=	rapid distortion theory
RPM	=	revolutions per minute
SPL	=	sound pressure level
u_{rms}	=	velocity fluctuations in the streamwise (x) direction
U_∞	=	freestream velocity
U_1	=	velocity of the flow before the contraction
U_2	=	velocity of the flow at the rotor plane
v_{rms}	=	fluctuation velocities in the radial (y) direction
$VTOL$	=	vertical take-off and landing
x	=	streamwise direction of flow
y	=	radial direction of flow

II. Introduction

Recent breakthroughs in the research on lightweight materials and electric engines have fostered rapid growth in the development of small vehicles to be employed for unmanned aerial recognition or urban air services [1]. While the variety of the vehicle design solutions is very broad, all the configurations share the necessity to operate in urban environments, most often characterized by very limited and confined space and by turbulent inflow conditions [2]. For these reasons, vertical take-off and landing (VTOL) configurations with propellers driven by electric engines have been the most popular choice in the market of the available design solutions so far. Indeed, the redundancy of the propulsive units guarantees safety and controllability, with each engine typically responding in real-time to adapt to the change of incoming flow [3]. These conditions pose a challenge from an acoustic modeling perspective [4], as both aerodynamic and acoustic performances directly impact the deployment feasibility of all the various configurations.

The problem of the interaction of incoming turbulence with a propeller and the consequent noise generation can be investigated by decomposing it into two different mechanisms: the first is related to the streamtube contraction, while the second one is due to the interaction with the airfoil. Prandtl [5] was the first to analyze the behavior of a turbulent flow accelerated in a contraction, showing that variations in the velocity components fluctuations are due to the stretching and shortening of the perpendicular vortex filaments. By indicating with the factor CR the ratio between the two velocities after and before the contraction, the variation of the velocity fluctuations was related to the alteration of the vortex filaments, which get elongated in the streamwise (x) direction and contracted in the (y) and (z) directions by a factor $\sqrt{CR}$. This distortion of the vorticity field causes the streamwise velocity component fluctuations to decrease and the normal components to increase. This work was followed by the one of Uberoi [6], whose experiments investigated the behavior of turbulence components for high contraction ratios (4:1, 9:1, and 16:1), confirming the predictions made by Prandtl. Jamaluddin et al. [7], in their study on the effect of turbulence intensity on the aeroacoustic characteristics of a propeller, analyzed the effect of the streamtube contraction on turbulence. They found out that the distortion of the upstream turbulence due to the streamtube contraction, causes the eddies to elongate and accelerate as they approach the propeller disk plane. Hunt [8] formulated the rapid distortion theory (RDT) to model the alteration of turbulence in rectilinear motion when it interacts with a cylinder. He identified two fundamental distortion mechanisms, discovering that the prevalence of one over the other can be determined through the ratio between the streamwise integral length scale of the turbulence L_{uu} and the radius of the cylinder a. For $L_{uu}/a \gg 1$ the prevailing distortion mechanism is due to the blockage imposed by the presence of the body, while for $L_{uu}/a \ll 1$ the distortion mechanism which dominates is determined by the deformation of the vorticity field due to the deflection of streamlines upstream and around the body. This theory has been first extended by Mish and Devenport [9] to airfoil configuration, proving that the distortion near the airfoil leading-edge is comparable to the one occurring for a cylinder with radius equal to the leading-edge radius, and then by Glegg et al. [10] to a rotor case.

The fact that small aerial vehicles operate mostly in strongly varying turbulent conditions, as the one characterizing urban environments, implies that acoustic performances are significantly affected by noise generated by turbulence

ingestion. Indeed, this justifyies the growing interest in the description and the modeling of this flow-induced noise source. A model to predict the broadband noise of a rotor caused by turbulence ingestion was proposed by Paterson and Amiet [11]. This model is derived from the theory developed for bidimensional flow conditions by Amiet [12], extended to take into account the rotating motion of the blades and the resulting effects on the noise generation. Paterson and Amiet [11] used the inflow turbulence statistics and rotor operating parameters to develop a theoretical approach to predict turbulence-ingestion noise spectra and directivity. The prediction method showed good agreement between theory and experiments, especially for high-frequency broadband noise. The primary limitation of this model is due to the insufficient description of the variation in turbulence characteristics along the radial direction and the effects of streamtube contraction. Indeed, the theory models incoming turbulence using a canonical turbulence spectrum, such as the von Karman one [13], hence neglecting the distortion experienced by turbulence as it approaches the rotor.

The present study intends to investigate possible enhancement methodologies for low-fidelity modeling of inflow-turbulence noise in the case of propellers. The goal is to include the alteration of turbulence characteristics due to the acceleration caused by the rotor and to account for the variation of flow conditions and blade geometry in the radial direction. A novel correction of Amiet's model based on the strip theory has been proposed to take into account these effects. This approach has been compared to the original model formulated by Amiet [14] for rotor noise prediction. To this purpose, an experimental campaign has been carried out in the A-Tunnel of Delft University of Technology. Stereoscopic PIV and HWA measurements were performed to analyze the interaction of a propeller with a grid-generated turbulent flow. A microphone array was installed to provide acoustic data and validate the low-fidelity noise-prediction.

The paper is organized as follows. Details about the experimental set-up and the measurement techniques are reported in III, which also reports information about the two low-fidelity noise-prediction methods investigated. The results of the flow characterization and the acoustic measurements and prediction are presented in IV, with the conclusions drawn in V.

III. Methodology

A. Experimental setup

The experimental investigation was carried out in the A-tunnel of the Delft University of Technology, a vertical open-jet wind tunnel whose exit is placed in an anechoic chamber. The propeller used in this campaign, the same one used by Grande et al [15], is a benchmarked version obtained from an APC 9x6 blade, with a diameter D of 22.86 cm and a pitch of 15.24 cm. The diameter has been scaled up to $D = 30$ cm, and each profile has been reshaped with a NACA 4412 airfoil. It is operated at a chord-based Reynolds number of about 10.8×10^4 based on the 75 % of the blade. Turbulence is generated by means of a regular grid with a mesh size G of 100 mm, a bar width d of 10 mm and a thickness t of 5 mm. The grid was placed between the contraction section of the open-jet wind tunnel and a cylindrical nozzle with a constant cross-section, at a distance of 1 m from the propeller, as shown in figure 1. The rotational speed of the propeller was set equal to 6000 RPM for the current experiments, while the flow speed of the wind tunnel was set equal to $U_\infty = 9.5$ m/s, resulting in an advance ratio $J = 0.317$. The origin of the reference frame used has been considered coincident with the hub of the propeller, with the x axis in the streamwise direction, the y axis along the blade, and z axis defined according to the right-hand rule.

B. PIV Measurements

Stereoscopic PIV measurements have been conducted to study the inflow of the propeller. The flow is seeded with particles of 1 µm generated by a SAFEX Twin Fog generator, with SAFEX-Inside-Nebelfluid. The field of view is illuminated using a Quantel Evergreen EVG00200 Nd:YAG laser, which delivers 200 mJ of energy per pulse with a maximum repetition rate of 15 Hz. Two LaVision sCMOS cameras with 2560x2160 pixels were employed for the acquisition of the images. Each camera was equipped with a Scheimplfug adapter and an AF Micro Nikkor lens with a 105 mm focal length. The lenses were operated at $f_\# = 11$. The set-up is shown in Fig. 2, while the PIV acquisition and post-processing details are collected in Table 1. In the case with the propeller, the PIV acquisitions were made both sampling statistically uncorrelated snapshots, as well as phase-locked snapshots. 1000 image pairs were acquired for each one of these two acquisition configurations. A cross-correlation algorithm with a window deformation iterative multigrid [16] was used, yielding a final interrogation window size of 16×16 pixels with a 75 % overlap. The misalignment between the images captured by the two cameras is reduced by performing a self-calibration, implemented through a disparity correction [17]. This procedure allows a final average misalignment of 0.63 mm to be retrieved.

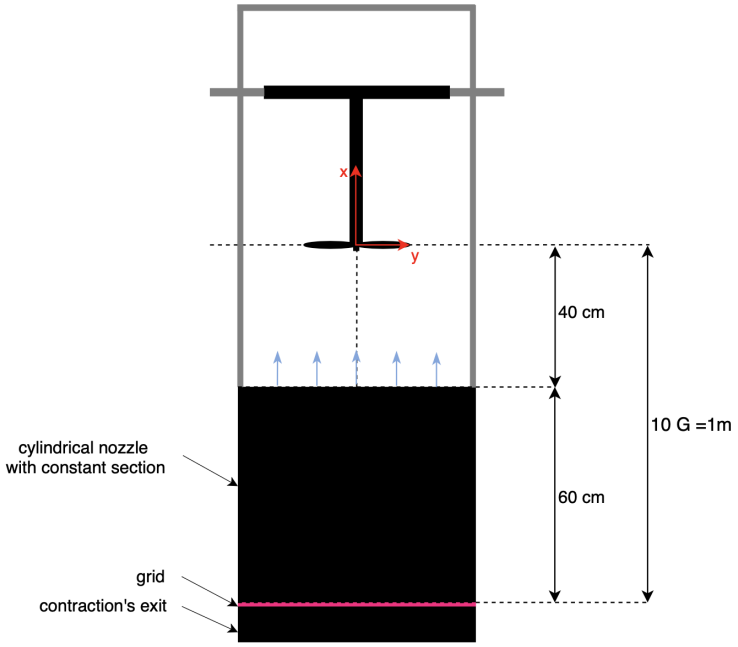

Fig. 1 Experimental set-up with the final part of the open-jet wind tunnel and the propeller.

Imaging parameters		PIV processing	
Camera	2 LaVision sCMOS	Software	LaVision Davis 10.2
Number of pixels [px]	2560×2160	Numbers of recordings	1000
Pixel size [µm]	6.5×6.5	Initial window size [px^2]	96×96
Focal length [mm]	105	Minimum window size [px^2]	16×16
$f_\#$	11		
FOV [cm^2]	$\approx 21 \times 25$		

Table 1 Details of PIV parameters

C. Hot-wire anemometry

HWA measurements were conducted to analyze the velocity field in the inflow of the propeller. The sampling grid consisted of 9 positions along the radial direction from the hub to the tip, separated by a distance equal to 12.5 % of the propeller radius, considered at 8 different distances from the rotor plane along the streamwise direction (see Fig. 3). A Dantec Dynamics type 55P11 probe was used for the acquisitions, driven by a constant temperature bridge and the hot wire is positioned to measure the velocity in the direction of the fluid flow. The acquisition frequency used was equal to 51.2 kHz and the acquisition time was equal to 60 s, which was deemed as sufficient to ensure statistical convergence of the turbulent statistics.

D. Acoustic Measurements

A microphone arc equipped with 7 G.R.A.S. 40 pH free-field microphones has been used. Each microphone has a diameter of 7 mm and works in a frequency range between 10 and 20 kHz up to a maximum sound pressure level (SPL) of 135 dB . The reference pressure is 20 µPa and the microphones have an integrated CCP preamplifier. Microphone signals have been recorded for a total of 120 s at 51.2 kHz.

The microphones were mounted on a 1.5 m radius arc with a minimum angular separation of 10° between two adjacent housings. These housings consist of a rod that can slide in the radial direction to allow the distance of the microphone from the center of the arc to be adjusted. Each microphone is positioned 1.3 m from the center of the propeller. Fig. 4 shows in detail the setup used to make the acoustic measurements. The acoustic measurements were conducted for two cases: with and without the propeller. The acoustic acquisitions without the rotor were conducted to identify

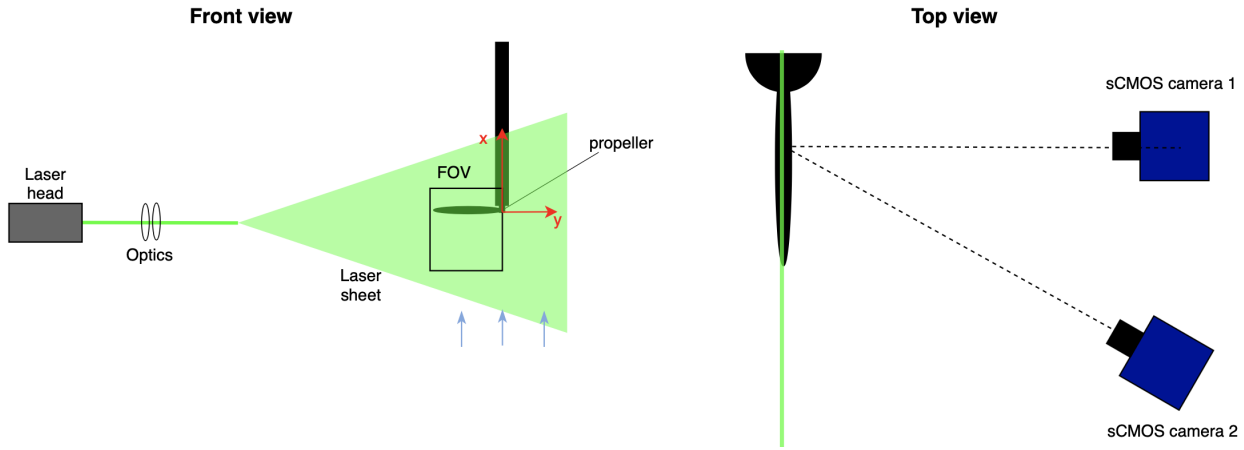

Fig. 2 Inflow Stereo PIV set-up

background noise sources, such as the turbulence-generating grid and the electric equipment controlling the PIV setup and the propeller.

E. Flow characterization

The incoming turbulence has been characterized in terms of turbulence intensity and integral length scale. The PIV and HWA measurements have been considered to calculate turbulence intensity, defined as in the following equation:

$$I = \frac{u_{rms}}{U_\infty} \tag{1}$$

where u_{rms} indicates the root-mean-square of the streamwise velocity fluctuations and $U_\infty = 9.5\,\mathrm{m/s}$ is the freestream velocity measured by a Pitot tube placed at the nozzle outlet.
As regards the integral length scale, two different methods have been employed, depending on the measurements taken into account. Indeed, the employment of the PIV acquisitions for the case without the propeller allows the integral length scale along a direction m to be calculated through the following expression

$$L_{ij}^{m} = \int_0^\infty R_{ij}(m)\mathrm{d}m = \int_0^\infty \frac{\overline{u_i(m)u_j(m+dm)}}{u_i(m)u_j(m+dm)}\mathrm{d}m, \tag{2}$$

with $R_{ij}(m)$ being the correlation calculated between the velocity components u_i and u_j. The overbar indicates the time-average operator and dm is the spatial increment.
A different methodology has been implemented to calculate the integral length scale using the HWA measurements. The following expression from Pope [18] has been employed to calculate the integral length scale from the frequency spectrum of the streamwise velocity component

$$L_{uu} = \frac{\pi E_{uu}(0)}{2\langle u^2 \rangle}. \tag{3}$$

where E_{uu} is the one-dimensional spectrum and $\langle u^2 \rangle$ is the variance of the streamwise velocity component.
The values of turbulence intensity and integral length scale resulting from the application of these expressions have been compared in IV to the empirical trends defined by Roach [19] for the decay of turbulence downstream of a grid.
Finally, the contraction ratio of the streamtube is calculated using statistically uncorrelated PIV acquisitions by means of the following expression.

$$\mathrm{CR} = \frac{U_2}{U_1} \tag{4}$$

where U_2 and U_1 are the mean values of the streamwise velocity component evaluated at $r/R = 0.75$. Specifically, U_2 was evaluated at the rotor plane $x/R = 0$ while U_1 was evaluated at $x/R = -0.8$ upstream of the propeller.

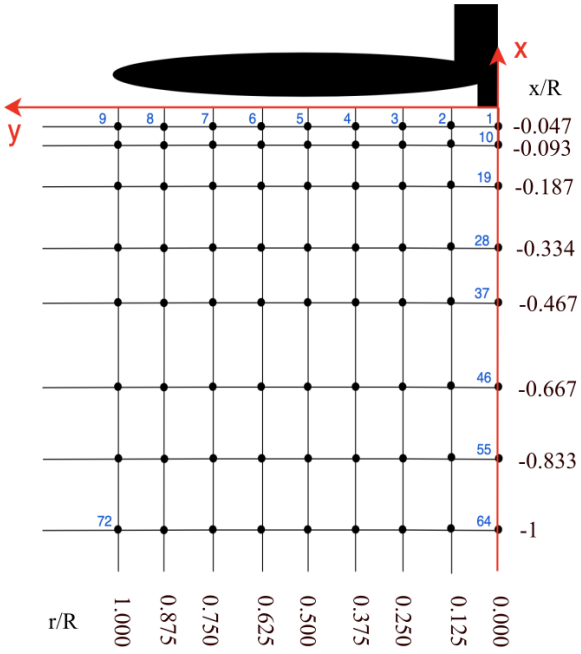

Fig. 3 HWA experimental set-up: coordinates of the positions where the flow was sampled.

F. Low-fidelity noise prediction

Two different formulations of Amiet's model for leading-edge noise prediction for the case of a propeller have been implemented and compared in the present work. The first one is the original model formulated by Amiet [14] for propeller noise, while the second one consists of a methodology proposed herein to account for radial variation of turbulence characteristics and blade geometry.

The characteristics and the differences between the two theoretical noise-prediction models are summarized below.

1. Amiet's model formulation for rotor noise prediction

The first model was directly derived from the basic Amiet's model for turbulence impingement noise scattering for an airfoil [12, 20, 21].

Amiet's model for an airfoil was extended to the rotor case with few modifications [11], [22], [14]. The theory for a rotor is derived from the assumption that the rotor blade can be considered composed of several airfoils moving in rectilinear motion. The results are then averaged over the azimuthal direction. The implementation of this averaging procedure is based on the assumption that the distance traveled by the blade during the turbulence impingement is negligible with respect to its full rotation. As output, the model provides the power spectral density as a function of the angular frequency ω_0 at the observer location $\boldsymbol{x} = (x, y, z)$, expressed as:

$$S_{pp}\left(\boldsymbol{x}, \omega_0\right) = \frac{B}{2\pi} \int_0^{2\pi} \left(\frac{\omega}{\omega_0}\right)^2 \left(\frac{\omega b x \rho_\infty}{c_\infty \sigma^2}\right)^2 \pi U_a d \left|\mathscr{L}\left(\bar{\lambda}, \bar{K}_y, M\right)\right|^2 b^2 \bar{u'}^2 \sum_{n=-\infty}^{+\infty} \Phi_{uu}\left(\lambda, K_x^n, K_y\right) \frac{\pi}{b^2 \bar{u'}^2 X} d\gamma \tag{5}$$

where B is the number of blades, ω is the angular frequency, and (ω/ω_0) is the Doppler-shift correction factor. $2b$ and $2d$ represent the airfoil chord and span, while ρ_∞ and c_∞ indicate the free-stream density and speed of sound, respectively. U_a is the advective velocity, $\bar{u'}^2$ is the free-stream turbulence intensity, γ is the azimuthal angle, K_y and K_x are factors that depend on geometrical information, on ω and on the wavenumbers in the streamwise direction [14]. $\mathscr{L}$ is the aeroacoustic transfer function and $\Phi_{uu}(\omega)$ is the turbulence spectrum, modeled using the von Karman turbulence spectrum expression.

It must be noticed that Eq. 5 is wrote using the same notation used by Amiet in [14], but the reference system is different in order to be consistent with the reference frame used in this paper and previously presented.

This model does not account for the geometrical characteristics of the rotor blade, considering that a single chord

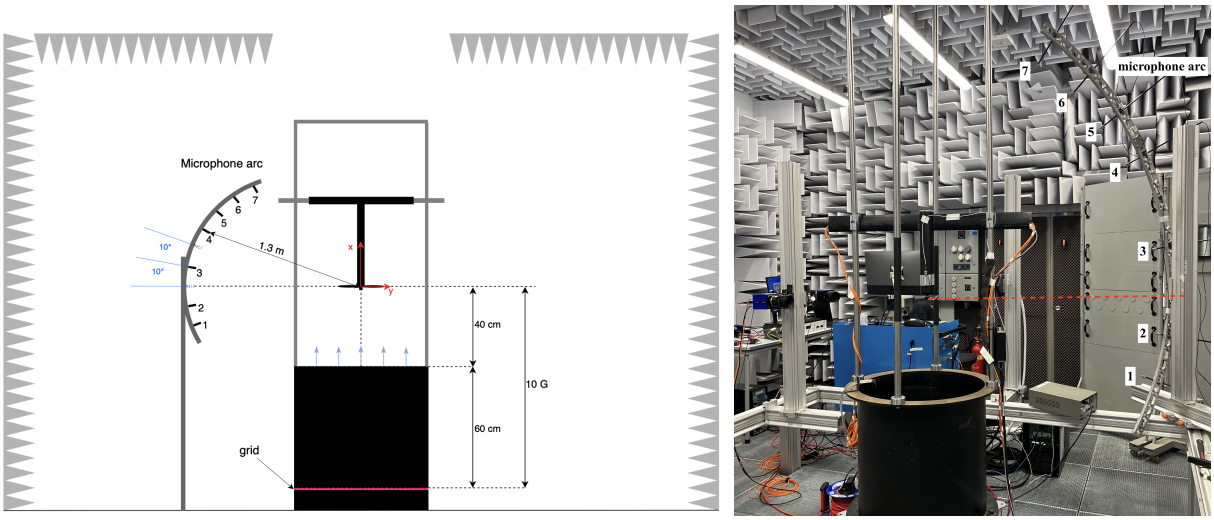

(a) (b)

Fig. 4 Acoustic set-up: a) schematic representation of the acoustic setup and b) image showing the experimental arrangement.

value is required as input. For the present implementation, the value of the chord chosen to perform the analysis is the one at 75% of the blade. Furthermore, turbulence is commonly modeled by means of canonical analytical expressions, such as the von Karman spectrum one, whose application requires only the value of turbulence integral length scale and intensity. Consequently, no alteration or directional variation of the turbulent velocity field is taken into account. In this case, the model has been applied using the turbulence characteristics sampled at the 75% of the blade, for several upstream distances from the propeller. The aim is to determine the distance from the propeller where the best noise spectrum approximation can be obtained.

2. Amiet's model modification to account for radial variation of blade geometry and flow characteristics

As previously explained, the geometrical characteristics of the blade and the alteration of the turbulent inflow are not taken into account in the original formulation of Amiet's model for leading-edge noise for the propeller case. The problem has been addressed by employing the strip theory [23, 24], which provides the overall noise generated by an airfoil as the summation of the noise generated by the strips resulting from a spanwise division of the surface. This allows the radial variation of the airfoil geometry and inflow conditions to be taken into account.

Christophe et al. [23] investigated two alternative approaches to calculate the contribution to the overall noise generated by each airfoil strip. In the first, indicated as "direct" approach, the noise emitted by the strips was obtained by considering each one of them as a very narrow-span airfoil and directly applying Amiet's model. In the second, referred to as "inverse" approach, the noise generated by the strip was obtained as the difference between the predictions yielded by Amiet's model for two very large span airfoils, whose difference in span corresponds to the width of the strip (figure 5). This methodology was shown to be more accurate at all frequencies and to allow the application of the following simplified formulation of Amiet's model, valid in the case of very large span

$$S_{pp}(x,0,z,\omega) = \left(\frac{\omega x \rho_0 b M}{\sigma^2}\right)^2 d\left|\mathscr{L}(z,K_z,0)\right|^2 l_y(\omega) S_{uu}(\omega). \tag{6}$$

In the previous expression, $l_y(\omega)$ indicates the spanwise coherence length, which will be related to the radial coherence of the flow in the case of the propeller, and $S_{uu}(\omega)$ is the PSD of the fluctuations of the velocity component perpendicular to the airfoil plane. In order to model this spectrum the von Karman expression has been applied, which requires as input the values of turbulent intensity and integral length scale. Specifically, the model has been applied by using the values of turbulence intensity and integral length scale evaluated at $x/R = -0.67$ upstream of the propeller. As regards the application of the strip theory, it has been implemented by dividing the blade into 8 strips.
The total contribution to the noise generated by the propeller is calculated as the sum of each single strip contribution,

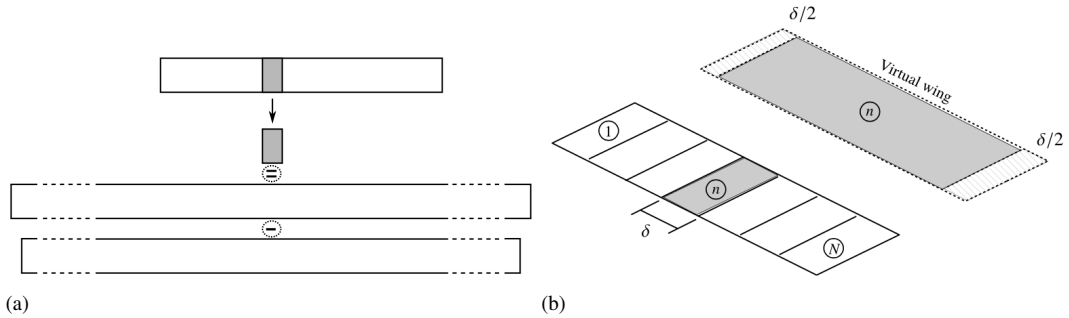

Fig. 5 Representation of the inverse strip method based on a combination of large span airfoils, from [23, 24]

as shown in Fig. 5(b):

$$S_{pp} = \sum_{n=1}^{N} \left(S_{pp}^{\infty} - S_{pp}^{(\infty - n)} \right) \tag{7}$$

where N is the number of strips considered.

This methodology has been extended to propeller applications by applying the same adjustments carried out in the original approach of [14], which account for the azimuthal average and the Doppler effect.

IV. Results

A. Flow characterization

The turbulent inflow is investigated for the cases with and without the propeller to identify the characteristics and alterations to consider to enhance the modeling of noise-generation mechanisms.

Fig. 6(a) shows the root-mean-square of the streamwise and radial velocity components along the streamwise direction for the case without the propeller at a radial position of $r/R = 0.75$. Both the HWA and the PIV measurements are reported in the figure. The other radial positions have been omitted since they exhibit very similar behavior to the one shown in the figure. An evident decrease in the streamwise direction characterizes the trends of the two components, in agreement with the empirical relation identified by Roach [19] predicting the decay of turbulence intensity downstream a grid. The HWA data, obtained by averaging all radial values at a fixed upstream distance, show a good agreement with the PIV measurements.

In Fig. 6(b), the turbulence length scale variation in the streamwise direction calculated from the PIV measurements for radial position $r/R = 0.75$ is shown for the acquisitions with grid and without the propeller. Also in this case, the length scale trend matches with the results from Roach [19].

The length scales obtained from the HWA measurements are reported in Table 2, for several radial locations. It is possible to notice that the upstream turbulence field is not perfectly homogeneous. Nevertheless, the radially-averaged value of the length scale evaluated from the HWA data is in agreement with the length scale calculated using the equation by Roach.

The streamtube contraction shown in Fig. 7 has been assessed to characterize the turbulent inflow in the case with the propeller. The contraction ratio CR, calculated using equation 4, is equal to 1.3 for a rotational speed of 6000 RPM.

Fig. 8 shows the trends of the root-mean-square of the streamwise and radial velocity components in the streamwise direction for the case with the propeller. Both the results of the PIV uncorrelated set of images and the phase-locked one have been reported in the figure. In the upstream region of the flow field, where it can be considered undisturbed by the presence of the propeller, u_{rms} and v_{rms} follow the trend of the empirical relation from Roach [19], until $x/R \approx$ -0.3 and $x/R \approx$ -0.15 for u_{rms} and v_{rms}, respectively. Beyond this distance, u_{rms} and v_{rms} undergo a sudden increase. In this region, the trend of the two quantities are primarily affected by the streamtube contraction and the turbulence distortion due to the interaction of the incoming eddies with the propeller blades. However, spurious effects affecting the PIV acquisition and post-processing, such as the blade movement and the laser reflections, could also affect this trend.

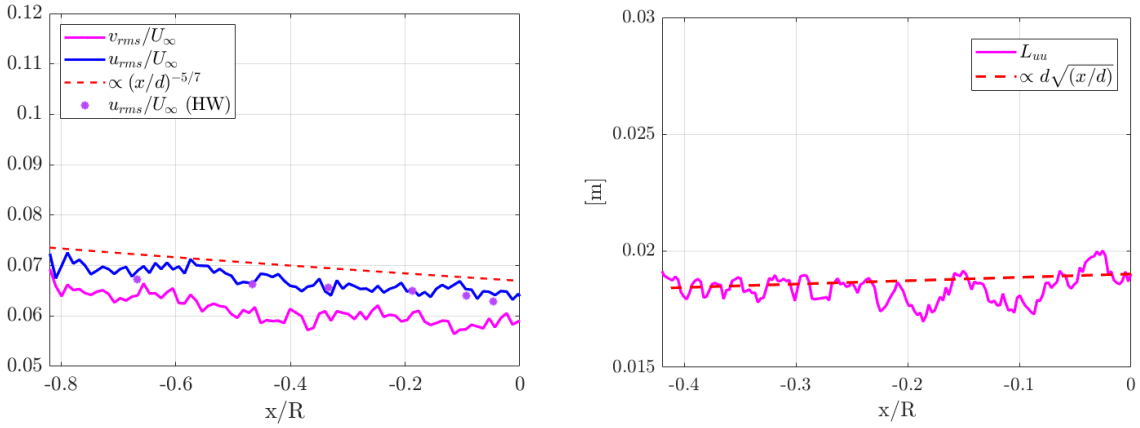

Fig. 6 Turbulent inflow characterization in the case without the propeller in terms of a) root-mean-square of the streamwise and the radial velocity components, normalized with respect to U_∞, along the streamwise direction at fixed radial position $r/R = 0.75$ and b) integral length scale evolution along the streamwise direction at radial position $r/R = 0.75$. The trend of the root-mean-square of the velocity fluctuations has been compared with the empirical formula $(x/d)^{-5/7}$ from Roach [19]

.

r/R [-]	L_{uu} [m]	$\overline{L_{uu}}$ [m]	L_{Roach} [m]
0.0	0.015		
0.25	0.023		
0.50	0.014	0.017	0.019
0.75	0.020		
1.00	0.012		

Table 2 Integral length scale evaluated from HWA data at streamwise position $x/R = 0.67$ upstream of the propeller for different radial positions in the case without the propeller. Radially-averaged value and and Roach prediction included as a reference.

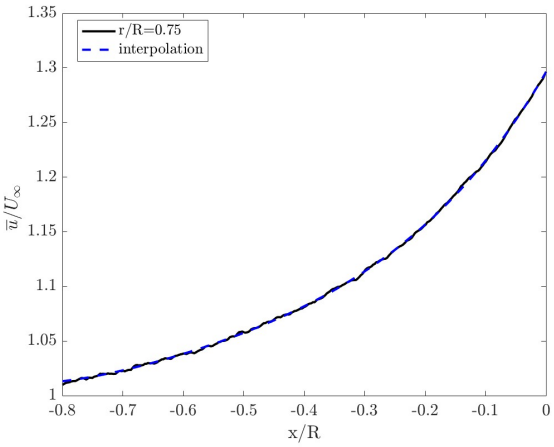

Fig. 7 Streamtube contraction for a radial position of $r/R = 0.75$, evaluated between a position $x/R = -0.8$ upstream of the propeller and the rotor plane $x/R = 0$.

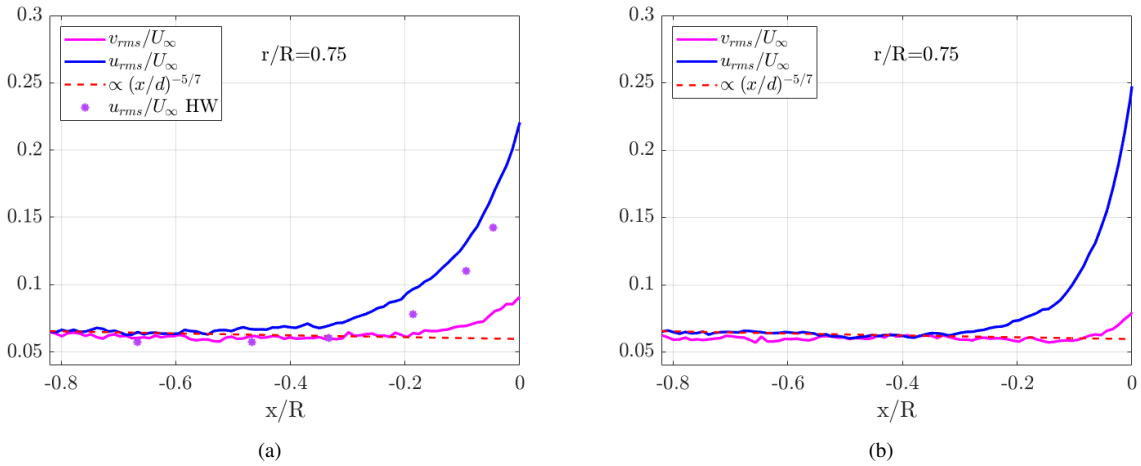

Fig. 8 Root-mean-square of the streamwise and the radial velocity components at fixed radial position $r/R = 0.75$, normalized with respect to U_∞ - a) uncorrelated set of images and HWA measurements; b) phase-locked set of images.

Despite these physical mechanisms are very difficult to decouple and investigate individually, some observations can be drawn from the comparison between the two plots for the statistically uncorrelated measurements and the phase-locked ones. Indeed, the comparison between Fig. 8(a) and Fig. 8(b) shows that the increase of the velocity components fluctuations for the phase-locked case is higher than in the statistically uncorrelated one. This is probably due to the fact that in the phase-locked case the blade lays in the laser sheet, causing the influence of the propeller on the observed turbulent fluctuations to be maximized. Even though laser reflection also affects the values of u_{rms} and v_{rms}, it is possible to infer that the presence of the propeller has a major impact on the alteration of the statistical characteristics of the upstream turbulence, also prevailing on the influence of the streamtube contraction.

It must be noticed that, differently from the findings of Uberoi [6] about the alteration of turbulence characteristics occurring in a contraction, a decrease of the streamwise velocity component fluctuation has not been detected in the present case. This can be attributed both to the predominant influence of the blade passage and the small value of the contraction ratio, significantly smaller than the lowest one investigated by Uberoi (equal to 4). This result confirms that in the present configuration the alteration of the incoming turbulence is mostly caused by the interaction with the blade rather than by the streamtube contraction effects.

B. Acoustic analysis and low-fidelity noise-prediction models implementation

The acoustic investigation entails the comparison between the results provided by the low-fidelity noise-prediction methods and the experimental measurements, which have been characterized to analyze the different sources contributing to the overall emitted noise.

Fig. 9 reports the SPL measured by the microphone at an azimuthal position of 70° (microphone 7) from the rotor plane for the cases with and without the propeller. In this latter configuration, noise is mostly generated by the turbulence-generating grid and the propeller motor. This is confirmed by this comparison, which indeed shows that most of the noise contributions at low frequencies, until a value of $f/BPF \approx 0.8$, and at the highest frequencies, from a value of $f/BPF \approx 5.5$, is due to the presence of the motor. Consequently, it can be inferred that the frequency range where the propeller noise contribution prevails is $0.8 < f/BPF < 5.5$.

In order to carry out a more reliable comparison with the low-fidelity broadband-noise predictions, the experimental spectra have been filtered by means of a moving average convolution to smooth out the tones. The result of this procedure is shown in Fig. 9.

The comparison between the filtered experimental acoustic spectra and the ones provided by the original formulation of Amiet's model is shown in Fig. 10(a). The low-fidelity method has been applied using as input the values of turbulence intensity extracted at several distances upstream of the propeller, summarized in table 3, and for a single radial position of $r/R = 0.75$. Turbulence intensity was obtained using the PIV phase-locked analysis data (Fig. 8(b)).

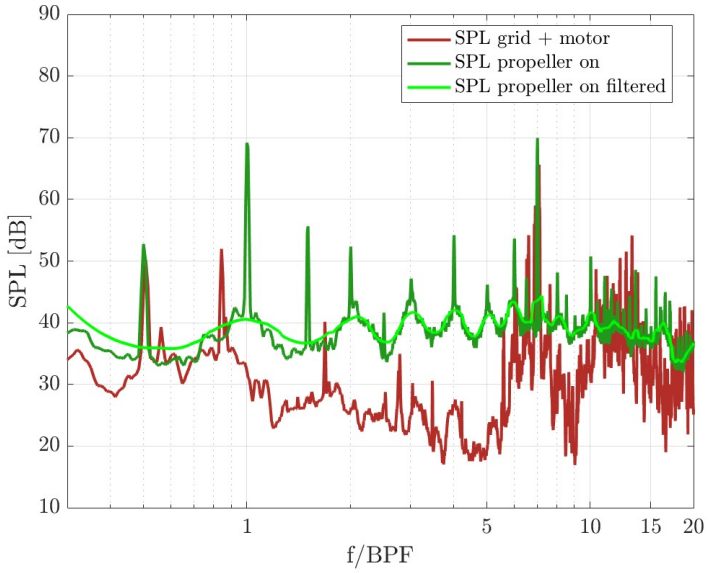

Fig. 9 Comparison between the SPL spectra of propeller noise, motor noise with grid installed, propeller noise filtered. All the spectra are acquired by the microphone 7

position	x	x/R
	[m]	[-]
1	-0.007	-0.047
2	-0.014	-0.093
3	-0.028	-0.187
4	-0.1	-0.67

Table 3 Positions upstream of the propeller where turbulence intensity has been extracted to be used as input to the Amiet's model for noise prediction.

The length scale used in all the cases is the one computed employing HWA measurements for a radial position of $r/R = 0.75$, equal to $L_{uu} = 0.020$ m (see Table 2). The value of the chord chosen as input ($c = 0.0225$ m) of the model has also been considered at a radial position of $r/R = 0.75$. The noise prediction has been calculated for an observer placed in the same position of microphone 7 (see Fig. 4). The investigation is focused on the frequency range where propeller noise prevails, i.e. between $f/BPF \approx 0.8$ and $f/BPF \approx 5.5$, as previously explained.

The comparison between the experimental and the predicted noise spectra indicates that the low-fidelity model developed by Amiet provides the best match by considering the turbulence inputs at a distance x/R =-0.047. This is the minimum upstream distance from the propeller studied in this analysis. As the distance from the propeller increases, greater differences are shown between the model and the experiments, since the spectra are strongly influenced by the value of the turbulence intensity. The discrepancy between the noise prediction and the experimental measurement has been quantified by calculating the overall sound pressure level (OASPL), calculated by performing the integral of each curve in the frequency range of interest. These values are summarized in Table 4, which also reports the difference between the OASPL of the measured far-field noise and the predicted one.

The results of the application of the low-fidelity model accounting for the radial variation of airfoil geometry and turbulence characteristics are shown in Fig. 10(b) in terms of SPL. The observer position taken into account to apply the modified Amiet's model is coincident with the position of microphone 7.

x [m]	OASPL [dB]	ΔOASPL [dB]	OASPL (Exp.) [dB]
−0.007	65.9	3.5	69.4
−0.014	62.9	6.5	
−0.028	59.9	9.5	
−0.100	58.6	10.8	

Table 4 OASPL for a frequency range of 0.8 < f/BPF < 5.5, and differences between the experimental OASPL and the OASPL of each curve.

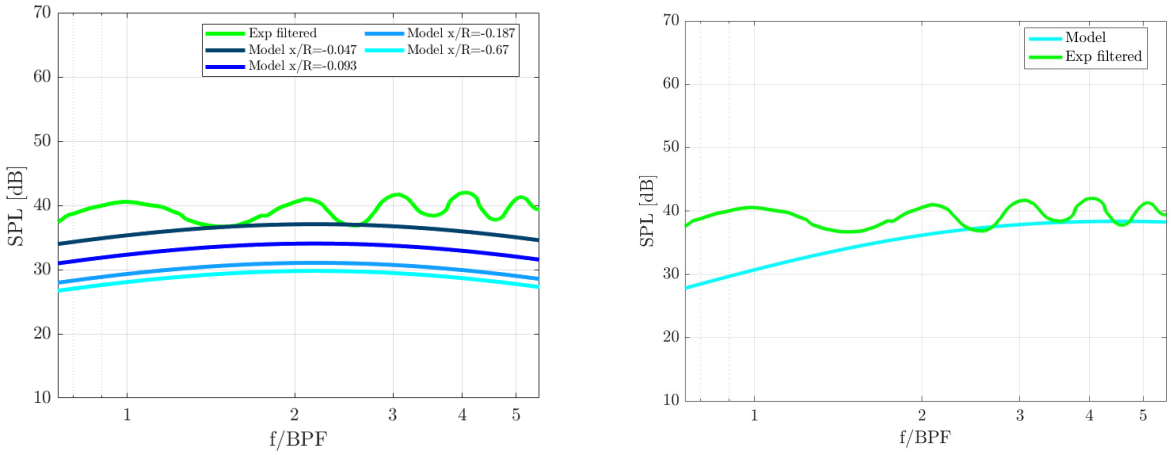

Fig. 10 Comparison between the SPL spectrum of the experimental acquisition, filtered with the moving average filter, and the predicted broadband noise SPL spectra a) First model: radial position of r/R =0.75 and for upstream positions of $x/R = -0.047, -0.093, -0.187, -0.67$ and b) Second model for an upstream position of $x/R = -0.67$.

This model provides a good noise prediction by considering the turbulence characteristics in a region upstream of the propeller, where the flow can be considered undisturbed by the presence of the propeller itself. So, only the variation of turbulence characteristics along the blade, in the radial direction, is considered in this model, and not the variation of turbulence due to the distortion caused by the propeller. This is because the implementation of this further step would require a more comprehensive modification to the formulation of the model proposed by Amiet.
The difference between the OASPL of the filtered experimental noise signal and the one of the predicted noise signal is equal to 2.5 dB, proving that this approach yields a more accurate prediction with respect to the other noise-prediction method. This can be attributed to the enhanced description of the blade geometry and the flow characteristics, suggesting that their variation in the radial direction can significantly affect noise generation in the case of propellers.

V. Conclusions

An analytical and experimental investigation into turbulence distortion of a low Reynolds number propeller was conducted to investigate the effects of turbulence characteristics on noise generation and modeling.

The campaign has been carried out in the anechoic open-jet wind tunnel of Delft University of Technology (A-Tunnel), using a rectangular grid to generate a turbulent inflow for the propeller. Flow measurements were performed by means of Stereoscopic PIV and hot-wire anemometry, while 7 microphones were placed along an arc for the acoustic characterization, with and without the propeller.

The influence of the streamtube contraction induced by the propeller was found not to have a remarkable impact on the turbulence intensity of the velocity components. This can be attributed to the relatively small value of the contraction

ratio and to the predominant effect of the motion of the propeller blades.

Two different analytical noise prediction models, based on Amiet's theory for leading-edge noise prediction, were implemented to account for turbulence alteration in the low-fidelity modeling. The first model implemented the original formulation of Amiet for the propeller case, which requires a position in the flow field to be specified to define the inflow conditions to use as input. The second model applied the inverse strip theory to account for the radial variation of the propeller geometry and the turbulence characteristics. The predicted broadband noise spectra provided by these models were compared with the one obtained experimentally in a frequency range of $0.8 < f/BPF < 5.5$, where the major contribution to the noise emitted is due to the propeller. The tones in the experimental spectrum were smoothed out using a moving average filter.

The models were applied using as input the turbulence intensity, provided by the PIV phase-locked analysis, and the turbulence length scale, calculated using the HWA measurements, at different distances from the rotor plane. As regards the first model, the best agreement between the predicted and the experimental spectra (Δ OASPL = 3.5 dB) is achieved for the minimum distance from the propeller plane considered in this study, $x/R = -0.047$. Concerning the second model, the flow conditions were evaluated at a distance of $x/R = -0.67$, where the flow can be considered undisturbed by the presence of the propeller itself. For that case, the Δ OASPL between the predicted spectrum and the experimental one is equal to 2.5 dB. Thus, a more accurate noise prediction can be obtained with the second model: the aerodynamic and acoustic response to the incoming perturbation, indeed, varies along the blade depending on the geometric characteristics of the profile and the alteration undergone by turbulence in the interaction with the propeller.

Further efforts are required to develop a more robust methodology than the one proposed in this study. In particular, a more thorough description and modeling of turbulence distortion in the interaction with an airfoil and a spinning blade is necessary. This would allow the prediction of the variation of turbulence characteristics knowing only the upstream flow characteristics and the propeller geometry and performances, leading hence to a significant enhancement of the state-of-the-art of low-fidelity prediction of leading-edge noise.

Acknowledgments

The authors would like to acknowledge Edoardo Grande and Luc van Beek for their help during the acquisition campaign and Tercio L. Pereira and Hugo Bento for their help and suggestions during the data post-processing.

References

[1] Ahmed, F., Mohanta, J. C., Keshari, A., and Yadav, S., P., "Recent Advances in Unmanned Aerial Vehicles: A Review," *Arabian Journal for Science and Engineering*, 2022.

[2] Giersch, S., El Guernaoui, O., Raasch, S., Sauer, M., and Palomar, M., "Atmospheric flow simulation strategies to assess turbulent wind conditions for safe drone operations in urban environments," *Journal of Wind Engineering and Industrial Aerodynamics*, 2022.

[3] Kim, D. H., Perry, T. A., and Ansell, J. P., "A review of Distributed Electric Propulsion for Air Vehicle Technology." *AIAA/IEEE Electric Aircraft Technologies Symposium (EATS)*, 2018.

[4] Jamaluddin, N. S., Celik, A., Baskaran, K., Rezgui, D., and Azarpeyvand, M., "Aeroacoustic Performance of Propellers in Turbulent Flow," *AIAA AVIATION 2021 FORUM*, 2021.

[5] Prandtl, L., "Herstellung einwandfreier Luftstrome (Windkanale)," *Handbuch der Exp, Physik, Leipzig, (Translated in NACA TM no. 726.)*, 1932.

[6] Uberoi, M., "Effect of Wind-Tunnel Contraction on Free-Stream Turbulence," *Journal of the Aeronautical Sciences*, Vol. 23, No. 8, 1956, p. 754–764.

[7] Jamaluddin, N. S., Celik, A., Baskaran, K., Rezgui, D., and Azarpeyvand, M., "Experimental analysis of a propeller noise in turbulent flow," *Physics of Fluids*, Vol. 35, No. 7, 2023, p. 075106.

[8] Hunt, C. R., J., "A theory of turbulent flow round two-dimensional bluff bodies," *Journal of Fluid Mechanics*, 1973, p. 625–706.

[9] Mish, P., and Devenport, W., "An experimental investigation of unsteady sur- face pressure on an airfoil in turbulence—Part 2: Sources and prediction of mean loading effects," *Journal of Sound and Vibration*, Vol. 296.3, 2006, p. 447–460.

[10] Glegg, S., Kawashima, E., Lachowski, F., and Devenport, W., "Propeller Noise: Inflow Distortion In a Non Axisymmetric Flow," 2013.

[11] Paterson, W., R., and Amiet, K., R., "Noise of a model helicopter rotor due to ingestion of isotropic turbulence," *Journal of Sound and Vibration*, 1982.

[12] Amiet, R., "Acoustic radiation from an airfoil in a turbulent stream," *Journal of Sound and Vibration*, 1975, pp. 407–420.

[13] von Kármán, T., and Lin, C. C., "On the Concept of Similiarity in the Theory of Isotropic Turbulence," *Rev. Mod. Phys.*, 1949.

[14] Amiet, R., "Noise produced by turbulent flow into a rotor: theory manual for noise calculation," *ASA Contractor report 181788*, 1989.

[15] Grande, E., Romani, G., Ragni, D., Avallone, F., and Casalino, D., "Aeroacoustic investigation of a propeller operating at low Reynolds numbers," *American Institute of Aeronautics and Astronautics*, Vol. 60.2, 2022, pp. 860–871.

[16] Scarano, F., and Riethmuller, M., "Advances in iterative multigrid PIV image processing," *Experiments in Fluids*, Vol. 29, 2012, pp. S051–S060. https://doi.org/10.1007/s003480070007.

[17] Willert, C., "Stereoscopic digital particle image velocimetry for application in wind tunnel flows," *Measurement Science and Technology*, Vol. 8, 1997, pp. 1465 – 1479. URL https://api.semanticscholar.org/CorpusID:250772454.

[18] Pope, S., *Turbulent flows*, Cambridge University Press, 2000.

[19] Roach, P. E., "The generation of nearly isotropic turbulence by means of grids," *International Journal of Heat and Fluid Flow*, 1987.

[20] Amiet, K., R., Egolf, G., C., and Simonich, C., J., "Noise produced by turbulent flow into a rotor: Users manual for noise calculation," *Nasa report*, 1989.

[21] Paterson, W., R., and Amiet, K., R., "Acoustic radiation and surface pressure characteristics of an airfoil due to incident turbulence," *AIAA Aeroacoustics conference,*, 1976.

[22] Amiet, K., R., "Noise due to rotor-turbulence interaction," *NASA Conference Publication 2052,*, 1978.

[23] Christophe, J., Anthoine, and Moreau, S., "Amiet's theory in spanwise-varying flow conditions," *AIAA Journal*, Vol. 47, No. 3, 2009, pp. 788–790.

[24] Miotto, R., Wolf, W., and de Santana, L., "Leading-Edge Noise Prediction of General Airfoil Profiles with Spanwise-Varying Inflow Conditions," *AIAA Journal*, 2018.